



LAWRENCE  
LIVERMORE  
NATIONAL  
LABORATORY

# Samarium-neodymium chronology and Rubidium-Strontium systematics of an Allende calcium-aluminum-rich inclusion with implications for $^{146}\text{Sm}$ half-life

N. E. Marks, L. E. Borg, I. D. Hutcheon, B. Jacobsen, R. N. Clayton

August 25, 2014

Earth and Planetary Science Letters

## **Disclaimer**

---

This document was prepared as an account of work sponsored by an agency of the United States government. Neither the United States government nor Lawrence Livermore National Security, LLC, nor any of their employees makes any warranty, expressed or implied, or assumes any legal liability or responsibility for the accuracy, completeness, or usefulness of any information, apparatus, product, or process disclosed, or represents that its use would not infringe privately owned rights. Reference herein to any specific commercial product, process, or service by trade name, trademark, manufacturer, or otherwise does not necessarily constitute or imply its endorsement, recommendation, or favoring by the United States government or Lawrence Livermore National Security, LLC. The views and opinions of authors expressed herein do not necessarily state or reflect those of the United States government or Lawrence Livermore National Security, LLC, and shall not be used for advertising or product endorsement purposes.

1  
2 ***Title: Samarium-neodymium chronology and Rubidium-Strontium***  
3 **systematics of an Allende calcium-aluminum-rich inclusion with implications**  
4 **for  $^{146}\text{Sm}$  half-life**

5  
6 **Authors:** N. Marks<sup>1\*</sup>, L.E. Borg<sup>1</sup>, I.D. Hutcheon<sup>1</sup>, B. Jacobsen<sup>1</sup>, R.N. Clayton<sup>2</sup>.

7 **Author affiliations:**

8 <sup>1</sup>Lawrence Livermore National Laboratory, 7000 East Avenue L-231, Livermore, CA 94551,  
9 USA.

10 <sup>2</sup>University of Chicago, 5640 S Ellis Ave, Chicago, IL 60637, USA.

11 \*Corresponding author: Naomi Marks, Lawrence Livermore National Laboratory, 7000 East  
12 Avenue L-231, Livermore, CA 94551, USA. 925-422-3853.

13 email: [marks23@llnl.gov](mailto:marks23@llnl.gov)

14 telephone: (408) 482-5676

15  
16 **Keywords:** CAIs, Sm-Nd, Rb-Sr, initial Solar System  $^{146}\text{Sm}/^{144}\text{Sm}$ ,  $^{146}\text{Sm}$  half-life  
17

18 **ABSTRACT**

19 Calcium-aluminum-rich inclusions (CAIs) are primitive objects that formed within the  
20 protoplanetary disk surrounding the young Sun. Recent Pb–Pb chronologic studies have  
21 demonstrated that CAIs are the oldest solar system solids, crystallizing 4567 Ma ago (Amelin et  
22 al., 2002; Connelly et al., 2012). The isotope systematics of CAIs therefore provide critical  
23 insight into the earliest history of the Solar System. Although Sm–Nd and Rb–Sr  
24 geochronometers are highly effective tools for investigating cosmochemical evolution in the  
25 early Solar System, previous studies of CAIs have revealed evidence for isotopically disturbed  
26 systems. Here we report new age data for Allende CAI Al3S4 derived from both the long-lived  
27 ( $^{147}\text{Sm}$ – $^{143}\text{Nd}$ ) and short-lived ( $^{146}\text{Sm}$ – $^{142}\text{Nd}$ ) isotopic systems. The  $^{147}\text{Sm}$ – $^{143}\text{Nd}$  chronometer  
28 yields an age of  $4560 \pm 34$  Ma that is concordant with  $^{207}\text{Pb}$ – $^{206}\text{Pb}$  ages for CAIs and indicates  
29 that the Sm–Nd system was not significantly disturbed by secondary alteration or  
30 nucleosynthetic processes. The slope of the  $^{146}\text{Sm}$ – $^{142}\text{Nd}$  isochron defines the Solar System  
31 initial  $^{146}\text{Sm}/^{144}\text{Sm}$  of  $0.00828 \pm 0.00044$ . This value is significantly different from the value of  
32 0.0094 determined by Kinoshita et al (2012). Ages recalculated from all published  $^{146}\text{Sm}$ – $^{142}\text{Nd}$   
33 isochron data using the traditional 103 Ma half-life and the initial  $^{146}\text{Sm}/^{144}\text{Sm}$  value determined  
34 here closely match Pb–Pb and  $^{147}\text{Sm}$ – $^{143}\text{Nd}$  ages determined on the same samples. In contrast,  
35 ages recalculated using the 68 Ma half-life determined by Kinoshita et al. (2012) and either of  
36 the initial  $^{146}\text{Sm}/^{144}\text{Sm}$  values are often anomalously old. This is particularly true for the  
37 youngest samples with  $^{146}\text{Sm}$ – $^{142}\text{Nd}$  isochron ages that are most sensitive to the choice of  $^{146}\text{Sm}$   
38 half-life used in the age calculation. In contrast to the Sm–Nd isotope system, the Rb–Sr system  
39 is affected by alteration but yields an apparent isochron with a slope corresponding to a much  
40 younger age of  $4247 \pm 110$  Ma. Although the Rb–Sr system in CAIs appears to be disturbed, the

41 initial  $^{87}\text{Sr}/^{86}\text{Sr}$  value determined from the isochron is  $0.698942 \pm 0.000008$ , and closely  
42 approximates estimates of the initial Solar System value. Although this isochron may be a  
43 mixing line, it might also record alteration on the Allende parent body in which Rb was added to  
44 the Al3S4 CAI that was initially largely devoid of Rb.

45

## 46 **1. Introduction**

47 Calcium-aluminum-rich inclusions formed in the protoplanetary disk surrounding the  
48 young Sun as a result of multiple transient heating events that thermally processed presolar dust  
49 and solar system condensates (Hood et al., 2009; Scott and Krot, 2007). In order to better  
50 understand the earliest history of the Solar System and the formation of CAIs, we investigated  
51 the chronometry of Allende CAI Al3S4 with improved methods for determining both absolute  
52 and relative ages. Isotopic analyses of the Sm–Nd and Rb–Sr systems were performed on CAI  
53 Al3S4 (also known as TS34), previously described by (Clayton et al., 1977), from the Allende  
54 CV3 carbonaceous chondrite. The Al3S4 CAI is an igneous type B inclusion in which the major  
55 minerals - melilite, clinopyroxene (Al, Ti-rich diopside), and anorthite exhibit chemical  
56 equilibrium (e.g. Simon et al. 1991).

57 The  $^{147}\text{Sm}$ – $^{143}\text{Nd}$  system has had relatively limited application in dating the earliest solar  
58 system materials, such as chondritic meteorites and CAIs. This is in part due to the limited  
59 spread in the  $^{147}\text{Sm}/^{144}\text{Nd}$  ratios present in these bulk samples that makes age determinations  
60 difficult. Analyses of minerals separated from several Allende and Efremovka CAIs have  
61 generally resulted in discrepant ages. For example, a four point isochron for Allende CAI Egg 2  
62 yielded an age of  $4.80 \pm 0.07$  Ga, whereas two point melilite-pyroxene tie-lines for Egg 6 and

63 Big Al yielded ages of  $4.80 \pm 0.18$  Ga and  $4.53 \pm 0.09$  Ga, respectively (Papanastassiou et al.,  
64 1987). Other Sm–Nd data reported for CAIs demonstrate clear evidence for isotopic  
65 disturbance, although some individual data points fall near a 4.55 Ga reference line  
66 (Bogdanovski and Jagoutz, 1999, Bogdanovski and Jagoutz, 1997). Thus, with the exception of  
67 the two-point tie-line for Allende CAI Big Al by (Papanastassiou et al., 1987), all published Sm–  
68 Nd data for CAIs demonstrate evidence for isotopic disturbance. The relative paucity of Sm–Nd  
69 age investigations of CAIs reflects the difficulties associated with: 1) obtaining large,  
70 petrographically well characterized samples, 2) producing high purity mineral separates that  
71 exhibit substantial fractionation of Sm and Nd, and 3) obtaining sufficiently accurate isotopic  
72 ratios on very small amounts of Nd and Sm. This study is based on large mineral fractions from  
73 Allende CAI Al3S4 produced at the University of Chicago circa 1975 that allowed long duration,  
74 high intensity, multi-dynamic runs of Nd<sup>+</sup> (rather than NdO<sup>+</sup> as in previous studies) on the  
75 newest generation of thermal ionization mass spectrometer. This approach minimizes  
76 measurement errors, facilitates high precision <sup>142</sup>Nd/<sup>144</sup>Nd and <sup>143</sup>Nd/<sup>144</sup>Nd ratio determinations,  
77 and ultimately allowed us to obtain undisturbed Sm–Nd isotopic systematics for a CAI.

78 The alpha decay of short-lived radionuclide <sup>146</sup>Sm to <sup>142</sup>Nd has been used as a  
79 geochronometer for determining the chronology of Solar System formation and early planetary  
80 differentiation, and provides insights into *p*-process nucleosynthesis of solar <sup>146</sup>Sm (e.g. Caro,  
81 2011; Boyet et al., 2010; Wassurburg et al., 2006; Audouze and Schramm, 1972). The half-life  
82 of <sup>146</sup>Sm has been measured five times (Meissner et al. 1987; Friedman et al. 1966; Nurmia et al.,  
83 1964; Dunlavey and Seaborg, 1953), and includes a recent measurement by Kinoshita et al.,  
84 (2012). The currently adopted half-life, derived from the work of Friedman et al. (1966) and  
85 Meissner et al., (1987) is  $103 \pm 5$  Ma. Kinoshita et al., (2012) determined a value for the <sup>146</sup>Sm

86 half-life of  $68 \pm 14$  Ma based on alpha activity counting experiments. This value is outside  
87 analytical uncertainty of the traditional 103 Ma half-life changing the time scales derived from  
88 the isotopic system. The coherent  $^{146}\text{Sm}$ - $^{142}\text{Nd}$  isochron derived from mineral separates of CAI  
89 Al3S4 in this study, provides an independent evaluation of the  $^{146}\text{Sm}$  half-life.

90         There is abundant evidence for isotopic disturbance of the Rb–Sr system in Allende CAIs  
91 (Gray et al., 1973; Tatsumoto et al., 1976; Podosek et al., 1991; Moynier et al., 2010). Young  
92 model ages of CAIs have been interpreted to reflect disturbance of the Rb–Sr system after the  
93 formation of the CAIs but before  $\sim 3.6$  Ga, implying that alteration occurred on the Allende  
94 parent body at least 1 Ga after CAI formation. In addition to the Sm–Nd data, we also present  
95 Rb–Sr isotopic data that strongly implies a disturbance to the system during alteration on the  
96 Allende parent body.

## 97 **2. Materials and Methods**

98         Allende CAI Al3S4 is also known as TS-34 and has been studied extensively (Clayton et  
99 al., 1977; Beckett, 1986; Simon et al., 1991; Davis et al., 1992; Beckett et al., 2000). A  
100 photomicrograph produced by Clayton et al. (1977) is presented in Figure 1. Al3S4 is a relatively  
101 large CAI, measuring 1.2 cm at its maximum dimension. The petrography of Al3S4 was  
102 described in detail by Clayton et al. (1977). The CAI has a well-defined mantle of melilite with  
103  $\sim 38$  volume percent (vol %) clinopyroxene (Al, Ti-rich diopside) and  $\sim 4$  vol % spinel. The core  
104 contains approximately 14 vol % spinel, 32 vol % melilite, 46 vol % clinopyroxene,  $< 2$  vol%  
105 anorthite, and  $\sim 6$  vol% secondary phases (Beckett, 1986; Connolly et al., 2003). Melilite and  
106 pyroxene (Al, Ti-rich diopside) crystals in the interior range up to  $\sim 1$  mm in size and are  
107 surrounded by a 1.5 mm thick mantle composed primarily of melilite. Spinel crystals 40–150

108  $\mu\text{m}$  in size are included in all major phases throughout the CAI. Cracks and veins of alteration,  
109 typical of most Allende inclusions, are present throughout TS-34. Secondary minerals are  
110 primarily grossular, monticellite, and wollastonite (Beckett, 1986).

111 Allende CAI Al3S4 was separated into constituent phases by a combination of magnetic  
112 and heavy liquid separations, as well as hand-picking, at the University of Chicago (Clayton et  
113 al., 1977). Mineral fractions were prepared using two density separation steps. In the first,  
114 melilite and pyroxene-dominated fractions were prepared from a 100–300  $\mu\text{m}$  size fraction using  
115 a solution of density 3.26  $\text{g}/\text{cm}^3$ . The melilite and pyroxene-dominated fractions were further  
116 crushed to  $<50 \mu\text{m}$  and separated into melilite and pyroxene fractions by hand-picking. Two  
117 density separates of the bulk CAI above and below 3.26  $\text{g}/\text{cm}^3$  were also analyzed. The  
118 composition of the mineral fractions was determined by x-ray diffraction at the University of  
119 Chicago (Clayton et al., 1977) and confirmed by SEM/EDS at Lawrence Livermore National  
120 Laboratory. A brief description of the composition of the mineral fractions follows: 1) the  
121  $d<3.26 \text{ g}/\text{cm}^3$  fraction consists primarily of melilite with minor anorthite and secondary minerals;  
122 2) the  $d>3.26 \text{ g}/\text{cm}^3$  fraction consists of pyroxene and spinel; 3) the pyroxene fraction consists of  
123 pyroxene (Al, Ti-rich diopside), spinel, and perovskite, 4) the melilite + pyroxene fraction  
124 consists primarily of melilite with minor pyroxene, 5) the melilite fraction consists of melilite  
125 with minor anorthite, and 6) the fines fraction consists of a split of the fine-grained,  $<325$  mesh  
126 powder, produced during sieving of the sample in preparation for mineral separations. Although  
127 the mineralogy of this fraction was not determined it is likely to contain a disproportionate  
128 amount of fine-grained alteration minerals, making it somewhat more vulnerable to isotopic  
129 disturbance.

130 The five mineral and fines fractions were washed and sonicated in deionized water at  
131 LLNL for 10 minutes, and then digested in concentrated HF+HNO<sub>3</sub> using Parr bombs. Samples  
132 were heated to 150°C for 24 hours in the bombs. Samples were transferred from the bombs and  
133 underwent repeated dry downs in aqua regia until completely digested with no residual material  
134 remaining. Following dissolution, 5% aliquots were spiked with <sup>149</sup>Sm and <sup>150</sup>Nd tracers (97.7%  
135 and 97.8% purity, respectively). In order to minimize uncertainty on the <sup>87</sup>Rb/<sup>86</sup>Sr ratio  
136 associated with the Rb laboratory blank, the 95% fractions were spiked with <sup>87</sup>Rb and <sup>84</sup>Sr tracers  
137 (98.0% and 99.2% purity, respectively). Rubidium, strontium, and REE were purified using  
138 BioRad AG-50W-X8 cation exchange resin and 2N and 6N HCL. Samarium and neodymium  
139 were separated using 0.2M α-HIBA acid in pressurized quartz columns. Samples analyzed for  
140 Nd isotope composition were passed through these columns twice to reduce <sup>142</sup>Ce interferences  
141 on <sup>142</sup>Nd. Total procedural blanks were 35 pg Sm, 117 pg Nd, 9 pg Rb, and 35 pg Sr. Although  
142 the need to digest the samples using bombs resulted in blanks that were significantly higher than  
143 usual, the high abundances of Sr and REE in the samples makes the blank contributions to the  
144 total elemental budget unimportant (0.0034–0.014% for Sm, 0.0040–0.017% for Nd, 0.0001–  
145 0.0063% for Sr, and 0.054–0.010% for Rb) in all but one fraction. The pyroxene fraction had a  
146 Rb contribution from the blank of 1.3% and required a significantly larger correction.

147 Mass spectrometry was performed on a ThermoScientific Triton thermal ionization mass  
148 spectrometer at LLNL. Neodymium isotopic compositions and <sup>147</sup>Sm/<sup>144</sup>Nd ratios of individual  
149 mineral fractions were determined on separate aliquots of the mineral separates, alleviating the  
150 need for correcting Nd isotopic compositions for the contribution of the 97.8% <sup>150</sup>Nd tracer  
151 (Table 1). Neodymium and samarium were loaded on double zone refined Re filaments in 2N  
152 HCl. Samarium was corrected for internal mass fraction using <sup>147</sup>Sm/<sup>152</sup>Sm = 0.56083.

153 Neodymium was run in dynamic mode at high intensity (2.7–4.8V  $^{144}\text{Nd}$ ;  $10^{11}$  ohm amplifiers)  
154 for 510 to 1080 ratios (8 second integrations) for all but one fraction to obtain very high  
155 precision  $^{142}\text{Nd}/^{144}\text{Nd}$  and  $^{143}\text{Nd}/^{144}\text{Nd}$  ratios. The  $d < 3.26 \text{ g/cm}^3$  fraction was run at 1.3V  $^{144}\text{Nd}$   
156 ( $10^{11}$  ohm amplifier) for 130 ratios. Ratios were corrected for mass fractionation to  $^{146}\text{Nd}/^{144}\text{Nd}$   
157 = 0.7219 using an exponential law. Long term  $^{142}\text{Nd}/^{144}\text{Nd}$  and  $^{143}\text{Nd}/^{144}\text{Nd}$  ratios measured for  
158 the JNdi-1 neodymium isotopic reference (Tanaka et al., 2000) was  $1.141837 \pm 0.000007$  and  
159  $0.512101 \pm 0.0000007$  (2 stdev;  $N = 37$ ), respectively. This is in good agreement with the  
160 average values obtained on 7 JNdi-1 standards run during the course of this investigation which  
161 were  $1.141837 \pm 0.000005$  and  $0.512102 \pm 0.0000003$  (2 stdev). The cerium interference on  
162  $^{142}\text{Nd}$  is 12-24 ppm for all mineral fractions except for Mel-Pyx (75 ppm) and Pyx (1400 ppm).  
163 Rubidium and strontium data are presented in Table 2. Strontium was run on single zone refined  
164 Re filaments with a  $\text{Ta}_2\text{O}_5$  emitter suspended in  $\text{H}_3\text{PO}_4$ . Data were collected in static mode using  
165  $10^{12}$  ohm amplifiers on  $^{84}\text{Sr}$ ,  $^{86}\text{Sr}$  and  $^{87}\text{Sr}$ . Individual mass spectrometer runs were performed at  
166 2–5V  $^{88}\text{Sr}$  intensities ( $10^{11}$  ohm amplifier) and consisted of 200 cycles with 16.8 second  
167 integration times. Internal mass fractionation was corrected using  $^{86}\text{Sr}/^{88}\text{Sr} = 0.1194$ . Replicate  
168 analyses of the NBS-987 Sr standard during the course of this investigation yielded an external  
169 reproducibility corresponding to  $^{87}\text{Sr}/^{86}\text{Sr} = 0.710243 \pm 0.000009$  (2 stdev;  $N=12$ ). Note that all  
170 of the published Sr isotopic data used for comparison were renormalized to our long-term NBS-  
171 987 value of  $^{87}\text{Sr}/^{86}\text{Sr} = 0.710249 \pm 0.000009$  (2 stdev;  $N=49$ ). Rubidium was run on single  
172 zone refined Re filaments. Instrumental mass fraction was corrected using the NBS-984 external  
173 standard assuming an  $^{85}\text{Rb}/^{86}\text{Sr}$  of 2.593; the uncertainty of Rb fractionation was 0.5%, and was  
174 propagated through the total uncertainty of 1%.

175

176 **3. Results**

177 *3.1 Sm-Nd systematics*

178 The Sm-Nd isotopic data for the mineral separates from CAI Al3S4 are listed in Table 1 and are  
179 plotted Figures 1 and 2. The  $^{147}\text{Sm}/^{144}\text{Nd}$  ratios for the mineral fractions demonstrate significant  
180 variation ranging from 0.17076 for the melilite fraction to 0.23204 for the pyroxene fraction.  
181 The mineral fractions fall on or very close to a single correlation line on both  $^{147}\text{Sm}-^{143}\text{Nd}$  and  
182  $^{146}\text{Sm}-^{142}\text{Nd}$  isochron plots. The isochrons were plotted with *Isoplot 4.1* (Ludwig et al., 2009)  
183 and include all data, although the  $^{147}\text{Sm}-^{142}\text{Nd}$  isochron does exclude data for the fines fraction.

184 *3.2 Rb-Sr systematics*

185 The Rb-Sr isotopic data for the same mineral separates analyzed for Sm-Nd are listed in Table 2  
186 and plotted in Figure 3. The  $^{87}\text{Rb}/^{86}\text{Sr}$  ratios range from 0.0076 for the melilite to 0.071 for the  
187 density >3.26 separate. The mineral separates plot on a single correlation line with an MSWD of  
188 1.4. The  $^{84}\text{Sr}/^{86}\text{Sr}$  ratios ( $\epsilon^{84}\text{Sr}$ ) of the mineral separates are listed in Table 2. The  $^{84}\text{Sr}/^{86}\text{Sr}$  ratios  
189 of the mineral separates have  $\epsilon^{84}\text{Sr}$  values ranging from 0.51 for the density separate >3.26 to  
190 1.34 for the pyroxene separate, with a mean  $\epsilon^{84}\text{Sr} = 1.08 \pm 0.30$ . The  $\epsilon^{84}\text{Sr}$  values are within error  
191 of the values measured in recent studies of nucleosynthetic anomalies in bulk CAIs (e.g.  
192 Brennecka et al., 2013; Hans et al., 2013; Moynier et al., 2010).

193

194 **4. Discussion**

195 *4.1 Sm-Nd ages of CAI crystallization*

196 The Sm–Nd isotopic data from Al3S4 form a well-defined linear array with a slope that  
197 reflects the crystallization age of the CAI (Table 1; Figs. 2 and 3). The  $^{147}\text{Sm}$ – $^{143}\text{Nd}$   
198 chronometer yields an age of  $4560 \pm 34$  Ma with a relatively small mean squared weighted  
199 deviation (MSWD) of 2.4. The agreement between the  $^{147}\text{Sm}$ – $^{143}\text{Nd}$  age and the accepted Pb–Pb  
200 age of  $4567.2 \pm 0.6$  Ma for CAIs (Amelin et al., 2002; Connelly et al., 2012; Amelin et al, 2010;  
201 Jacobsen et al., 2008; Bouvier and Wadhwa, 2010) provides strong evidence that the Sm–Nd  
202 isotopic system in Al3S4 has been minimally disturbed since the CAI cooled below the closure  
203 temperature for Sm and Nd diffusion. This age is concordant with the two-point melilite and  
204 pyroxene tie line age of  $4.53 \pm 0.09$  Ga reported for Allende CAI Big Al by Papanastassiou et al.  
205 (1987), but is more precise. Some evidence for disturbance of the Sm–Nd isotopic system in  
206 CAI Al3S4 is revealed by the fines fraction, however. This separate lies off the  $^{147}\text{Sm}$ – $^{143}\text{Nd}$   
207 isochron, but on the  $^{146}\text{Sm}$ – $^{142}\text{Nd}$  isochron (see below). This fraction was produced during initial  
208 crushing of the CAI and was separated from the other fractions during the sieving process. As a  
209 result, this fraction contains the finest-grained, most easily friable, component of the CAI and is  
210 expected to have a larger proportion of secondary minerals than the other mineral fractions. The  
211 initial  $^{143}\text{Nd}/^{144}\text{Nd}$  ratio derived from the isochron is  $0.506657 \pm 0.000043$  ( $\epsilon^{143}\text{Nd} = -0.34 \pm$   
212  $0.85$ ), and agrees with  $^{143}\text{Nd}/^{144}\text{Nd}$  ratios previously determined on primitive chondritic  
213 meteorites of  $0.506686 \pm 0.000070$  ( $\epsilon^{143}\text{Nd} = 0.24 \pm 1.4$ ; Bouvier et al., 2008) and  $0.50665 \pm$   
214  $0.00014$  ( $\epsilon^{143}\text{Nd} = -0.47 \pm 2.8$ ; Amelin and Rotenberg, 2004), but is more precise. The initial  
215  $^{143}\text{Nd}/^{144}\text{Nd}$  determined from CAI Al3S4 isochron is within uncertainty of the value of  $0.506674$   
216 ( $\epsilon^{143}\text{Nd} \equiv 0$ ) proposed by Jacobsen and Wasserburg (1980, 1984) for the CHondritic Uniform  
217 Reservoir (CHUR). This agreement confirms the current CHUR parameters, and provides

218 additional evidence that the Sm–Nd isotopic systematics of Al3S4 record the crystallization age  
219 of the sample.

220 The availability of relatively large mineral fractions allowed the first internal  $^{146}\text{Sm}$ –  
221  $^{142}\text{Nd}$  isochron for a CAI to be produced. The initial  $^{146}\text{Sm}/^{144}\text{Sm}$  ratio defined by the slope of  
222 the isochron is  $0.00828 \pm 0.00044$  (Fig. 3). This value is likely to be one of the most accurate  
223 representations of the initial  $^{146}\text{Sm}/^{144}\text{Sm}$  ratio of the Solar System, not only because CAIs are  
224 the earliest solids formed in the protoplanetary disk, but also because the linearity of the isochron  
225 provides assurance that the  $^{146}\text{Sm}$ – $^{142}\text{Nd}$  isotopic systematics are not disturbed. The initial  
226  $^{146}\text{Sm}/^{144}\text{Sm}$  ratio defined by the CAI isochron is in excellent agreement with the value of  $0.0085$   
227  $\pm 0.0007$  determined from basaltic eucrite meteorites by (Boyet et al., 2010), but differs  
228 significantly from the  $^{146}\text{Sm}/^{144}\text{Sm}$  ratio of  $0.0094 \pm 0.0005$  determined by (Kinoshita et al.,  
229 2012). The  $^{146}\text{Sm}/^{144}\text{Sm}$  ratios calculated by (Boyet et al., 2010) and (Kinoshita et al., 2012) are  
230 based on Sm–Nd isotopic measurements of the same set of eucrite samples but determined using  
231 the 103 Ma and 68 Ma  $^{146}\text{Sm}$  half-lives, respectively.

232 The  $^{146}\text{Sm}$ – $^{142}\text{Nd}$  isochron yields an initial  $^{142}\text{Nd}/^{144}\text{Nd}$  ratio of  $1.141496 \pm 0.000018$ .  
233 Relative to our terrestrial standard this corresponds to an  $\epsilon^{142}\text{Nd}$  value of  $-3.01 \pm 0.16$ . Initial  
234  $\epsilon^{142}\text{Nd}$  values for bulk Earth and chondritic meteorites are calculated using estimated bulk  
235  $^{147}\text{Sm}/^{144}\text{Nd}$  ratios that range from 0.1960 (Bouvier et al., 2008) to 0.1967 (Jacobsen and  
236 Wasserburg 1980, 1984; Amelin and Rotenberg, 2004) and  $^{142}\text{Nd}/^{144}\text{Nd}$  ratios determined on  
237 terrestrial standard and chondritic meteorites (e.g., Boyet et al., 2005), respectively. The  
238 estimated initial terrestrial  $\epsilon^{142}\text{Nd}$  value is  $-2.92 \pm 0.07$ , whereas the initial value inferred from  
239 chondritic meteorites is  $-3.13 \pm 0.07$ . Uncertainties include measurement uncertainties on  
240  $^{142}\text{Nd}/^{144}\text{Nd}$  ratios of  $\pm 0.000007$ . This analysis demonstrates that the initial  $^{142}\text{Nd}/^{144}\text{Nd}$  inferred

241 from the CAI isochron is intermediate between the value inferred for the Earth and chondritic  
242 meteorites, but is within analytical uncertainty of both.

243

### 244 *3.2 Role of nucleosynthetic anomalies in Sm–Nd chronometry*

245 Small nucleosynthetic anomalies in Sm and Nd have recently been reported in Allende  
246 CAIs by Brennecka et al. (2013). These anomalies have the potential to affect both the inferred  
247 Sm and Nd concentrations and the  $^{147}\text{Sm}/^{144}\text{Nd}$  ratios for the CAI mineral fractions because  
248 the  $^{150}\text{Nd}/^{144}\text{Nd}$  and  $^{149}\text{Sm}/^{152}\text{Sm}$  ratios in CAIs may not have (the assumed) terrestrial values.  
249 We addressed these effects using the average Sm and Nd isotopic compositions determined by  
250 Brennecka et al. (2013) on eleven un-spiked Allende CAIs to deconvolve our isotope dilution  
251 measurements. The magnitude of these corrections on the  $^{147}\text{Sm}/^{144}\text{Nd}$  ratios was approximately  
252 0.015%. Any isotopic anomalies, therefore, have no effect on the slope and only a extremely  
253 minor shift in the initial  $^{142}\text{Nd}/^{144}\text{Nd}$  ratio determined from the  $^{146}\text{Sm}$ - $^{142}\text{Nd}$  isochron.

254 Isotopic anomalies produced by *r*-, *s*-, and *p*-process nucleosynthesis could, in principle,  
255 cause the Sm-Nd isotopic systematics of CAIs to differ from the Sm-Nd isotopic systematics of  
256 other Solar System materials. Specifically, negative anomalies in the *p*-process isotope  $^{144}\text{Sm}$   
257 suggest that similar deficits could exist in other *p*-process isotopes such as  $^{146}\text{Sm}$ . However, it is  
258 difficult to quantitatively evaluate the magnitude of potential *p*-process anomalies in a  
259 radionuclide such as  $^{146}\text{Sm}$  because the proportion of  $^{146}\text{Sm}$  present in the molecular cloud is  
260 dependent on the time since it was produced in a supernova. Nevertheless, *p*-process anomalies  
261 in  $^{144}\text{Sm}$  are extremely small, ~2 parts in 10,000 (0.02%). A shift in the abundance of  $^{146}\text{Sm}$  by  
262 0.02% changes the initial  $^{146}\text{Sm}/^{144}\text{Sm}$  ratio by an amount encompassed by the analytical

263 uncertainty on the  $^{146}\text{Sm}/^{144}\text{Sm}$  ratio inferred from the slope of the  $^{146}\text{Sm}$ - $^{142}\text{Nd}$  isochron.  
264 Furthermore, the good agreement between the initial  $^{146}\text{Sm}/^{144}\text{Sm}$  ratio for the Solar System  
265 calculated from the Sm-Nd isotopic systematics of angrite (Lugmair and Galer, 1992; Nyquist et  
266 al. 1994) and eucrite meteorites (Boyet et al., 2010) suggest that all of these early Solar System  
267 materials are derived from a source with a common  $^{146}\text{Sm}/^{144}\text{Sm}$  ratio, and that differences  
268 in  $^{146}\text{Sm}/^{144}\text{Sm}$  due to nucleosynthesis cannot be distinguished with analytical uncertainty.

269         Although the initial  $^{142}\text{Nd}/^{144}\text{Nd}$  ratio determined from the Al3S4 isochron is similar to  
270 the values derived from both chondritic meteorites and bulk Earth, it is important to note that the  
271 abundances of the other stable Nd isotopes in CAIs are measurably different (Brennecka et al.,  
272 2013). The stable Nd isotopic compositions of the Al3S4 mineral fractions are presented in Table  
273 1 and permit nucleosynthetic effects to be evaluated for this sample. The  $^{145}\text{Nd}/^{144}\text{Nd}$   
274 and  $^{148}\text{Nd}/^{144}\text{Nd}$  ratios are lower than the corresponding terrestrial values by  $\sim 0.2$  epsilon units,  
275 whereas the  $^{150}\text{Nd}/^{144}\text{Nd}$  ratio is lower by  $\sim 1.0$  epsilon unit (Table 1), consistent with the  
276 magnitude of anomalies measured in eleven bulk Allende CAIs by Brennecka et al. (2013). -A  
277  $0.14 \pm 0.26$  epsilon unit correction for nucleosynthetic effects on  $^{142}\text{Nd}/^{144}\text{Nd}$  can be calculated  
278 using the  $^{148}\text{Nd}/^{144}\text{Nd}$  data measured on the mineral fractions and the correlation of  $^{148}\text{Nd}$ - $^{142}\text{Nd}$   
279 determined from primitive chondrites (Qin et a., 2011 and Boyet and Gannoun 2013). A  
280 correction of  $0.14 \pm 0.14$  epsilon units is calculated if the more precise  $^{148}\text{Nd}/^{144}\text{Nd}$   
281 measurements determined from bulk Allende CAIs by Brennecka et al (2013) are used. This  
282 implies that the initial  $^{142}\text{Nd}/^{144}\text{Nd}$  determined from the isochron reflects a minimum estimate for  
283 the bulk Nd isotopic composition of the Solar System. However, because the errors associated  
284 with the corrections are the same size as the corrections themselves, a more definitive constraint  
285 on the initial Nd isotopic composition of the solar System is not possible. It should be noted,

286 however, the small deviations in the initial  $^{142}\text{Nd}/^{144}\text{Nd}$  ratio of Al3S4 from the bulk Nd isotopic  
287 composition of primitive chondritic meteorites or bulk Earth will have no effect on the slope of  
288 the  $^{146}\text{Sm}-^{142}\text{Nd}$  isochron. Thus, differences between the  $^{146}\text{Sm}/^{144}\text{Sm}$  initial ratio calculated by  
289 Kinoshita et al. (2012) and the value determined from the Al3S4 isochron are not the result of  
290 nucleosynthetic processes that occurred prior to the formation of the Solar System.

291

### 292 *3.3 Evaluation of the $^{146}\text{Sm}$ half-life and initial $^{146}\text{Sm}/^{144}\text{Sm}$ ratio*

293 The accuracy of the new  $^{146}\text{Sm}$  half-life presented by (Kinoshita et al., 2012) cannot be  
294 directly evaluated using the Al3S4  $^{146}\text{Sm}-^{142}\text{Nd}$  isochron presented here because this isochron  
295 likely defines the initial  $^{146}\text{Sm}/^{144}\text{Sm}$  ratio of the Solar System. The disagreement between the  
296 initial  $^{146}\text{Sm}/^{144}\text{Sm}$  ratio determined by (Kinoshita et al., 2012) and the value determined by both  
297 (Boyet et al., 2010) and inferred from the CAI data presented here, however, suggests the 68 Ma  
298 half-life reported by Kinoshita et al. may be incorrect.

299 We evaluated the accuracy of the  $^{146}\text{Sm}$  half-life determined by Kinoshita et al. (2012) by  
300 comparing the Pb–Pb and  $^{147}\text{Sm}-^{143}\text{Nd}$  ages determined on meteorite and lunar samples with  
301  $^{146}\text{Sm}-^{142}\text{Nd}$  mineral isochron ages calculated for the same samples using the different  $^{146}\text{Sm}$   
302 half-lives. Table 3 presents  $^{146}\text{Sm}-^{142}\text{Nd}$  isochron ages calculated from available Sm–Nd data in  
303 the literature using both potential  $^{146}\text{Sm}$  half-lives and initial  $^{146}\text{Sm}/^{144}\text{Sm}$  ratios. Although the  
304 uncertainty on the 68 Ma half life is  $\pm 14$  Ma, and the uncertainty on the 103 Ma half life of  $\pm 5$   
305 Ma, these are not taken into account in this comparison because they are not typically included in  
306 the uncertainties of most published  $^{146}\text{Sm}-^{142}\text{Nd}$  ages. Figure 4 compares ages derived from the  
307  $^{146}\text{Sm}-^{142}\text{Nd}$  system with either Pb–Pb ages or  $^{147}\text{Sm}-^{143}\text{Nd}$  ages determined on the same

308 samples. Also plotted on Figure 4 is a 1:1 line illustrating concordance between the various  
309 chronometers. Lines are regressed through the age data to assess which  $^{146}\text{Sm}$  half-life and  
310 initial  $^{146}\text{Sm}/^{144}\text{Sm}$  most closely approximates the 1:1 line. Although there is significant scatter,  
311 this analysis permits the two half-lives to be evaluated within the context of the published Sm–  
312 Nd data. From Figure 4 it is apparent that a line regressed through all of the ages determined  
313 using the 103 Ma half-life and initial  $^{146}\text{Sm}/^{144}\text{Sm}$  of 0.00828 lies very close to the 1:1 line,  
314 whereas ages calculated using the 68 Ma half-life and either of the initial  $^{146}\text{Sm}/^{144}\text{Sm}$  values  
315 does not. The  $^{146}\text{Sm}$ – $^{142}\text{Nd}$  ages calculated using the 68 Ma half-life and initial  $^{146}\text{Sm}/^{144}\text{Sm}$  of  
316 0.0094 proposed by (Kinoshita et al., 2012) are very similar to those calculated using the initial  
317  $^{146}\text{Sm}/^{144}\text{Sm}$  ratio of 0.00828 measured in this investigation. Thus, the observation that the 103  
318 Ma half-life provides a better fit to the published age data is largely independent of the initial  
319  $^{146}\text{Sm}/^{144}\text{Sm}$  ratio assumed in the age calculation. The concordance between the  $^{146}\text{Sm}$ – $^{142}\text{Nd}$   
320 isochron ages calculated using  $^{146}\text{Sm}/^{144}\text{Sm} = 0.00828$  and  $^{146}\text{Sm}$   $t_{1/2} = 103$  Ma with Pb–Pb and  
321  $^{147}\text{Sm}$ – $^{143}\text{Nd}$  ages determined on the same samples implies that the 103 Ma half-life provides the  
322 most accurate representation of the  $^{146}\text{Sm}$  decay rate.

323 Note that the slopes of the regressions in Figure 4 are strongly dependent on four  
324 relatively young lunar sample ages. This observation stems from the inability of ancient samples  
325 to constrain the  $^{146}\text{Sm}$  half-life because the uncertainty on  $^{146}\text{Sm}$ – $^{142}\text{Nd}$  isochron slopes is large in  
326 comparison to the small difference between the isochron slopes derived from ancient samples  
327 and the initial Solar System  $^{146}\text{Sm}/^{144}\text{Sm}$  value. For example, the  $^{146}\text{Sm}$ – $^{142}\text{Nd}$  age for angrite  
328 LEW86010 recalculated from data presented by Nyquist et al. (1994) using the 68 Ma half-life  
329 and initial  $^{146}\text{Sm}/^{144}\text{Sm}$  ratio of 0.0094 is  $4546^{+11}_{-12}$  Ma, in general agreement with the  $4557.8 \pm$   
330 0.2 Ma Pb–Pb age for this meteorite (Galer and Lugmair, 1996; Amelin, 2008). However, an

331 essentially identical age of  $4554^{+17}_{-19}$  Ma is derived using the 103 Ma half-life. It is therefore  
332 necessary to examine the  $^{146}\text{Sm}$ – $^{142}\text{Nd}$  ages of relatively young samples for which measurably  
333 different amounts of  $^{142}\text{Nd}$  ingrowth has occurred since the beginning of the Solar System in  
334 order to evaluate the accuracy of the two  $^{146}\text{Sm}$  half-lives. Ages calculated for relatively young  
335 lunar ferroan anorthosites 60025 and 60016, as well as lunar troctolite 76535 and lunar norite  
336 77215 (Borg et al., 2011; Marks et al., 2014; Borg et al., 2013; Carlson et al. 2013) using the 68  
337 Ma  $^{146}\text{Sm}$  half-life and initial Solar System  $^{146}\text{Sm}/^{144}\text{Sm}$  of 0.0094 are  $4406^{+19}_{-22}$  Ma,  $4377^{+38}_{-62}$   
338 Ma,  $4392^{+19}_{-24}$  Ma, and  $4412^{+38}_{-64}$  respectively. These ages are significantly older than the  
339 corresponding Pb–Pb and  $^{147}\text{Sm}$ – $^{143}\text{Nd}$  ages of these samples:  $4359 \pm 3$  Ma (60025),  $4300 \pm 32$   
340 Ma (60016),  $4306 \pm 11$  Ma (76535), and  $4283 \pm 23$  Ma (77215). We find far better agreement  
341 between the absolute ages of these lunar samples and the  $^{146}\text{Sm}$ – $^{142}\text{Nd}$  ages calculated using the  
342 103 Ma  $^{146}\text{Sm}$  half-life and initial Solar System  $^{146}\text{Sm}/^{144}\text{Sm}$  of 0.00828. These calculations  
343 yield ages of  $4322^{+27}_{-33}$  Ma for 60025,  $4298^{+57}_{-94}$  Ma for 60016,  $4301^{+29}_{-36}$  Ma for 76535, and  
344  $4351^{+57}_{-96}$  Ma for 77215. This analysis supports the accuracy of the 103 Ma half-life of  $^{146}\text{Sm}$ .

345

### 346 *3.4 Rb–Sr isotopic systematics*

347 Rubidium–strontium isotopic compositions were determined for the same separates of  
348 CAI Al3S4 analyzed for Sm–Nd (Table 3). The Rb–Sr data form a highly linear array (MSWD  
349 of 1.3) on an isochron plot, yielding an age of  $4247 \pm 110$  Ma and an initial  $^{87}\text{Sr}/^{86}\text{Sr}$  ratio of  
350  $0.698942 \pm 0.000008$  using an  $^{87}\text{Rb}$  decay constant of  $1.402 \times 10^{-11}$  (Begemann et al., 2001; Fig.  
351 5). The fines fraction does not fall along the isochron, suggesting the presence of isotopically

352 disturbed minerals in this fraction. The relatively large uncertainty in age reflects the limited  
353 spread in  $^{87}\text{Rb}/^{86}\text{Sr}$  ratios relative to the precision of  $^{87}\text{Sr}/^{86}\text{Sr}$  ratio measurements ( $\sim 0.0007\%$ ;  
354  $2\sigma$ ). The initial  $^{87}\text{Sr}/^{86}\text{Sr}$  ratio determined from the isochron is slightly lower than the Solar  
355 System initial  $^{87}\text{Sr}/^{86}\text{Sr}$  ratio of  $0.69887 \pm 0.00002$  determined by (Gray et al., 1973) and the  
356 value of  $0.69891 \pm 0.00002$  determined by (Podosek et al., 1991) from analyses of Allende CAIs  
357 (both values are renormalized to the  $^{87}\text{Sr}/^{86}\text{Sr}$  for the NBS standard value used here of  $0.710243$   
358  $\pm 0.000009$ ). Like previous Sr isotopic data from CAIs, the initial Sr isotopic composition  
359 determined from the Al3S4 data is slightly lower than the initial  $^{87}\text{Sr}/^{86}\text{Sr}$  ratios determined for  
360 the angrite meteorites Angra Dos Reis ( $0.698978 \pm 0.000004$ ) and LEW86010 ( $0.698971 \pm$   
361  $0.000008$ ) by (Hans et al., 2013; Nyquist et al., 1994). The value inferred from Al3S4 is also  
362 substantially lower than the Basaltic Achondrite Best Initial (BABI)  $^{87}\text{Sr}/^{86}\text{Sr}$  ratio of  $0.699083 \pm$   
363  $0.000055$  (Papanastassiou and Wasserburg, 1969) or the recently revised BABI value of  
364  $0.698970 \pm 0.000028$  (Hans et al., 2013). The fact that the measured initial  $^{87}\text{Sr}/^{86}\text{Sr}$  ratio lies  
365 very near, or slightly below, previous estimates for the initial Solar System value demonstrates  
366 that Al3S4 formed very early in Solar System history in an environment that was essentially Rb-  
367 free. Note that the data for Al3S4 show an apparent  $^{84}\text{Sr}$  excess, similar to the excesses observed  
368 in several recent studies of Allende CAIs (Table 2; Brennecka et al., 2013; Hans et al., 2013;  
369 Moynier et al., 2010). Furthermore, it has been argued that the  $^{84}\text{Sr}$  anomaly is an artifact of an  
370 unobserved anomaly on  $^{86}\text{Sr}$  that stems from the fractionation correction procedure that assumes  
371  $^{86}\text{Sr}/^{88}\text{Sr}$  is equal to the terrestrial value of  $0.1194$ . Applying a correction of  $0.62 \pm 0.35$  epsilon  
372 units (half of the  $^{84}\text{Sr}$  anomaly value from Hans et al., 2013) to the initial  $^{87}\text{Sr}/^{86}\text{Sr}$  of CAI Al3S4  
373 shifts the initial  $^{87}\text{Sr}/^{86}\text{Sr}$  from  $0.698942$  to  $0.699004$ . The adjusted value is in good, but not

374 perfect, agreement with the Solar System initial value estimated from CAIs and primitive  
375 meteorites by Hans et al. (2013).

376 Previous work has provided strong evidence for isotopic disturbance of the Rb–Sr system  
377 in Allende CAIs (Gray et al., 1973; Tatsumoto et al., 1976; Podosek et al., 1991; Moynier et al.,  
378 2010). Gray et al., (1973) determined Rb–Sr model ages ( $T_{\text{BABI}}$ ) on a number of Rb-rich  
379 aggregates ( $^{87}\text{Rb}/^{86}\text{Sr} > 0.3$ ) and found them to be as young as 3.6 Ga. They interpreted these  
380 ages to reflect disturbance of the Rb–Sr system later than 3.6 Ga, implying that alteration  
381 occurred on the Allende parent body at least 1000 Ma following CAI formation. Late formation  
382 of some secondary phases found in CAIs is consistent with the absence of radiogenic  $^{26}\text{Mg}^*$   
383 produced by in-growth of short-lived  $^{26}\text{Al}$  (Jacobsen et al., 2011). It is possible that the  
384 radiogenic  $^{87}\text{Sr}$  in the Al<sub>3</sub>S<sub>4</sub> mineral fractions is derived almost exclusively from secondary  
385 phases (i.e. sodalite and nepheline). Variations in  $^{87}\text{Rb}/^{86}\text{Sr}$  ratios could reflect both the  
386 abundances of these phases in the various separates as well as the concentration of Sr in the  
387 primary CAI minerals in the separates.

388 The Rb–Sr isochron has several possible interpretations. On one hand, it might reflect  
389 mixing of a small amount of a Rb-rich contaminant into mineral fractions initially devoid of Rb  
390 and consequently having a non-radiogenic Sr isotopic composition at 4567 Ma. Analysis of  
391 Allende bulk matrix material by Tatsumoto et al. (1976), however, demonstrate that this material  
392 falls significantly above the 4.25 Ga slope line regressed through the Al<sub>3</sub>S<sub>4</sub> mineral fractions.  
393 Allende bulk matrix, therefore, cannot serve as the contaminant. Likewise, Wetherill et al.  
394 (1973) analyzed Rb–Sr systematics from a fine-grained, sodium-rich Allende CAI with a high  
395 Rb/Sr ratio ( $^{87}\text{Rb}/^{86}\text{Sr} = 0.521$ ); the data plot well above the 4.25 Ga line. In fact, a line  
396 regressed through the Al<sub>3</sub>S<sub>4</sub> mineral fractions and the fine-grained Allende inclusion analyzed

397 by Wetherill et al. (1973) has a slope corresponding to  $4642 \pm 34$  Ma (MSWD = 12). It therefore  
398 seems likely that the behavior of the Rb–Sr system in fine-grained inclusions primarily reflects  
399 fractionation of Rb/Sr occurring soon after (or during) the formation of fine-grained inclusions.  
400 Thus, simple mixing of matrix materials that have Rb–Sr isotopic systematics similar to other  
401 components in the Allende meteorite cannot produce the 4.25 Ga isochron. Instead, material  
402 with higher Rb/Sr or lower  $^{87}\text{Sr}/^{86}\text{Sr}$  is required. Another interpretation involves addition of a  
403 laboratory contaminant. This scenario seems unlikely, however, because several Allende CAIs,  
404 analyzed in different laboratories, all demonstrate similar Rb–Sr isotopic systematics (Gray et al.,  
405 1973; Tatsumoto et al., 1976; Podosek et al., 1991). Perhaps the most feasible contaminant  
406 would be derived from Allende matrix but having a Rb/Sr ratio modified during metamorphism.

407 A final possibility is that the disturbance of the Rb–Sr isotopic system involves the  
408 addition of a small amount of very high Rb/Sr material into Al3S4 at  $\sim 4.25$  Ga. In this case Rb  
409 would have been introduced in a single event or over a relatively short time interval to an object  
410 previously devoid of Rb. Due to the absence of  $^{87}\text{Rb}$ , the Sr isotopic composition of minerals in  
411 Al3S4 would not have evolved significantly from the initial Solar System  $^{87}\text{Sr}/^{86}\text{Sr}$  value. If this  
412 scenario is correct, an extremely small amount (i.e., less than 100 ng) of Rb was added to the  
413 CAI as a result of metamorphism on the Allende parent body at  $\sim 4.25$  Ga. Secondary minerals,  
414 such as grossular, monticellite, sodalite, nepheline, and wollastonite, forming during  
415 metamorphism would have incorporated this Rb over a time period of hours to days. Radiogenic  
416 growth of  $^{87}\text{Sr}$  in these minerals would then yield a Rb–Sr age reflecting the time of parent body  
417 metamorphism. However, if the alteration process added significant amounts of Sr, as well as  
418 Rb, the linear array on the Rb–Sr plot defined by the mineral fractions would reflect mixing,  
419 rather than ingrowth of  $^{87}\text{Sr}$ . -In any case, the Rb–Sr age of 4.25 Ga suggests that there was a late

420 metamorphic event on the Allende parent asteroid, although the timing of this event is not  
421 uniquely defined.

### 422 *3.5 Chronology and metamorphism in CAIs*

423         The observation that the event that introduced Rb into the CAI did not significantly affect  
424 other chronometers provides insight into metamorphic processes on the Allende parent asteroid.  
425 The extremely low concentration of Rb in primary CAI minerals (<0.06–0.23  $\mu\text{g/g}$ ; Table 2)  
426 makes the Rb–Sr system extremely sensitive to late addition of small amounts of Rb. In contrast,  
427 Sm and Nd have significantly higher abundances in CAIs and are refractory elements, difficult to  
428 redistribute by metamorphic processes that effectively mobilize Rb and other more soluble  
429 elements. As a consequence, the Sm–Nd system has preserved a record of crystallization in CAI  
430 Al3S4. The Pb–Pb chronometer, like the Rb–Sr chronometer, is susceptible to contamination  
431 during metamorphism. However, sequential leaching processes are commonly applied for Pb–  
432 Pb chronometry, specifically to remove secondary Pb added during metamorphism. As a result,  
433 Pb–Pb ages of CAIs are derived from mineral fractions that do not contain significant amounts of  
434 extraneous Pb and are consequently less likely to reflect the effects of post-crystallization  
435 metamorphic processes. In summary, crystallization ages of moderately altered CAIs may be  
436 obtained using the Pb–Pb, Al–Mg, and Sm–Nd systems, but are unlikely to be obtained from the  
437 Rb–Sr isotopic system.

438

## 439 **4. Conclusions**

440 A  $^{147}\text{Sm}$ – $^{143}\text{Nd}$  age of  $4560 \pm 34$  Ma and an initial  $^{143}\text{Nd}/^{144}\text{Nd}$  of  $0.506657 \pm 43$  was determined  
441 for mineral fractions from the coarse-grained type B Allende inclusion Al3S4. This is the first  
442 age determined on a CAI that is not based on an assumed initial isotopic composition of the  
443 Solar System and is in good agreement with previously determined Al–Mg and Pb–Pb ages of  
444 CAIs. This concordance, combined with an initial  $^{143}\text{Nd}/^{144}\text{Nd}$  value similar to initial Solar  
445 System values from bulk meteorites (e.g., Bouvier et al., 2008; Amelin and Rottenberg, 2004;  
446 Jacobsen and Wasserburg, 1980), suggests that the Sm–Nd isotopic systematics of Al3S4 are  
447 minimally disturbed. A  $^{146}\text{Sm}$ – $^{142}\text{Nd}$  isochron with a slope corresponding to an initial  
448  $^{146}\text{Sm}/^{144}\text{Sm} = 0.00828 \pm 0.00044$  was obtained from the same mineral fractions. This initial  
449 ratio is in excellent agreement with the initial  $^{146}\text{Sm}/^{144}\text{Sm}$  value of the Solar System determined  
450 by Boyet et al. 2010, but measurably different from the value of 0.0094 calculated by Kinoshita  
451 et al. (2012) using the newly determined 68 Ma  $^{146}\text{Sm}$  half-life. All published  $^{146}\text{Sm}$ – $^{142}\text{Nd}$   
452 isochron ages were recalculated using both the 68 Ma and 103 Ma half-lives in conjunction with  
453 the initial  $^{146}\text{Sm}/^{144}\text{Sm}$  of 0.00828 determined here and the value of 0.0094 proposed by  
454 Kinoshita et al. (2012). This evaluation demonstrates that  $^{146}\text{Sm}$ – $^{142}\text{Nd}$  ages calculated using the  
455 103 Ma half-life and initial  $^{146}\text{Sm}/^{144}\text{Sm}$  of 0.00828 reproduce Pb–Pb and  $^{147}\text{Sm}$ – $^{143}\text{Nd}$  ages  
456 determined on the same samples significantly better than ages calculated using the 68 Ma half-  
457 life and either of the initial  $^{146}\text{Sm}/^{144}\text{Sm}$  values. This analysis is strongly based on several young  
458 lunar samples because these samples yield initial  $^{146}\text{Sm}/^{144}\text{Sm}$  ratios lying significantly outside  
459 analytical uncertainty of the Solar System initial value. Revision of the  $^{146}\text{Sm}$  half-life to the  
460 previous value of 103 Ma has significant implications for the timing of terrestrial, lunar, and  
461 Martian planetary silicate mantle differentiation, requiring planetary differentiation to have  
462 occurred somewhat later than would be predicted from calculations based on the 68 Ma value.

463 The Rb–Sr systematics of CAI Al<sub>3</sub>S<sub>4</sub> are clearly disturbed, but form a well defined linear array  
464 with a slope corresponding to 4.25 Ga. The significance of this age is not clear, although it could  
465 represent the age of alteration on the Allende parent asteroid if metamorphism involved the  
466 addition of a very small amount of Rb, and essentially no Sr, into Al<sub>3</sub>S<sub>4</sub>.

## 467 **Acknowledgements**

468 This contribution is dedicated to Toshiko K. Mayeda. Without her invaluable contributions this  
469 project would not have been possible. We thank T. Kleine and two anonymous reviewers for  
470 valuable comments. This work was performed under the auspices of the US Department of  
471 Energy by Lawrence Livermore National Laboratory under contract number DE-AC52-  
472 07NA27344. The portion of the work performed at Lawrence Livermore National Laboratory  
473 was supported by NASA Origins of Solar Systems grant NNH10AO05I (P.I. Hutcheon) and  
474 NASA Cosmochemistry grants NNH12AT841 (P.I. Borg) and NNH10AO48I (P.I. Hutcheon).

475

## 476 **References**

477

- 478 Audouze, J., Schramm, D. N., 1972. 146Sm: a Chronometer for p-Process Nucleosynthesis.  
479 Nature 237:447-449. doi:10.1038/237447a0
- 480 Amelin, Y., 2008. U–Pb ages of angrites. *Geochim. Cosmochim. Acta* 72, 221-232.
- 481 Amelin, Y., Kaltenbach, A., Iizuka, T., Stirling, C.H., Ireland, T.R., Petaev, M., Jacobsen, S.B.,  
482 2010. U–Pb chronology of the Solar System's oldest solids with variable <sup>238</sup>U/<sup>235</sup>U. *Earth*  
483 *Planet. Sci. Lett.* 300, 343-350.
- 484 Amelin, Y., Krot, A.N., Hutcheon, I.D., Ulyanov, A.A., 2002. Lead isotopic ages of chondrules  
485 and calcium-aluminum-rich inclusions. *Science* 297 1678-1683.
- 486 Amelin, Y., Rotenberg, E., 2004. Sm–Nd systematics of chondrites. *Earth Planet. Sci. Lett.* 223,  
487 267-282.
- 488 Amelin, Y., Wadhwa, M., Lugmair, G., 2006. Pb-Isotopic Dating of Meteorites Using <sup>202</sup>Pb-<sup>205</sup>Pb  
489 Double-Spike: Comparison with Other High-Resolution Chronometers. *Lunar Planet. Sci.*  
490 Conf. XXXVII, Houston, Texas. abstract #1970.

- 491 Beckett, J.R., 1986. The origin of calcium-, aluminum-rich inclusions from carbonaceous  
492 chondrites: An experimental study (Doctoral dissertation, University of Chicago, Depart.  
493 Geophys. Sci.).
- 494 Beckett, J.R., Simon, S.B., Stolper, E., 2000. The partitioning of Na between melilite and liquid:  
495 Part II. Applications to type B inclusions from carbonaceous chondrites. *Geochim.*  
496 *Cosmochim. Acta* 64, 2519–2534.
- 497 Begemann, F., Ludwig, K.R., Lugmair, G.W., Min, K., Nyquist, L.E., Patchett, P.J., Renee, P.R.,  
498 Shih, C.-Y., Villa, I.M., Walker, R.J., 2001. Call for an improved set of decay constants for  
499 geochronological use. *Geochim. Cosmochim. Acta* 65, 111-121.
- 500 Bogdanovski, O., Jagoutz, E., 1999. Samarium-neodymium isotopic systematics of CAIs from  
501 Efremovka and Allende meteorites. XXX Lunar and Planetary Science Conference, Houston  
502 Texas. abstract #1981.
- 503 Bogdanovski, O., Jagoutz, E., 1997 Sm-Nd isotopic system in Allende CAI's. XXVIII Lunar and  
504 Planetary Science Conference, Houston Texas. abstract #1798
- 505 Borg, L.E., Connelly, J.N., Boyet, M., Carlson, R.W., 2011. Chronological evidence that the  
506 Moon is either young or did not have a global magma ocean. *Nature*, 477, 70-72.
- 507 Borg, L.E., Connelly, J.N., Cassata, W., Gaffney, A.M., Carlson, R.W., Papanastassiou D. A.,  
508 Wasserburg J.G., Ramon, E., Lindvall, R., Bizarro, M., 2013. Evidence for widespread  
509 magmatic activity at 4.36 GA in the Lunar Highlands from young ages determined on  
510 troctolite 76535. XLIV Lunar and Planetary Science Conference, Houston Texas. abstract  
511 #1563.
- 512 Bouvier, A., Vervoort, J.D., Patchett, P.J. 2008. The Lu–Hf and Sm–Nd isotopic composition of  
513 CHUR: constraints from unequilibrated chondrites and implications for the bulk composition  
514 of terrestrial planets. *Earth Planet Sci. Lett.* 273, 48-57.
- 515 Bouvier, A., Wadhwa, M., 2010. The age of the Solar System redefined by the oldest Pb–Pb age  
516 of a meteoritic inclusion. *Nature Geosci.* 22, 637-641.
- 517 Boyet, M., Carlson, R.W., 2005. <sup>142</sup>Nd evidence for early (> 4.53 Ga) global differentiation of  
518 the silicate Earth. *Science*, 309, 576-581.
- 519 Boyet, M., Carlson, R.W., Horan, M., 2010. Old Sm-Nd ages for cumulate eucrites and  
520 redetermination of the solar system initial <sup>146</sup>Sm/<sup>144</sup>Sm ratio. *Earth Planet. Sci. Lett.* 291, 172-  
521 181.
- 522 Boyet M., Gannoun A. 2013. Nucleosynthetic Nd isotope anomalies in primitive enstatite  
523 chondrites. *Geochim et Cosmochim Acta* 121, 652-666.
- 524 Brennecka, G.A., Borg, L.E., Wadhwa, M., 2013. Evidence for supernova injection into the solar  
525 nebula and the decoupling of r-process nucleosynthesis. *Proc. Natl. Acad. Sci.* 110, 17241-  
526 17246.
- 527 Brennecka, G. A., Borg, L. E., Wadhwa, M. 2012. Combined Stable Isotope Signatures in  
528 Allende CAIs: The Nucleosynthetic Conundrum. In *Lunar and Planetary Institute Science*  
529 *Conference Abstracts* (Vol. 43, p. 2006).
- 530 Brennecka, G. A., Borg, L. E., Wadhwa, M. 2011. Barium, Neodymium, and Samarium Isotopic  
531 Composition of CAIs: Nucleosynthetic Anomalies?. *LPI Contributions*, 1639, 9036.

- 532 Brennecka, G. A., Weyer, S., Wadhwa, M., Janney, P. E., Zipfel, J., Anbar, A. D. 2010.  
 533  $^{238}\text{U}/^{235}\text{U}$  variations in meteorites: Extant  $^{247}\text{Cm}$  and implications for Pb-Pb dating. *Science*,  
 534 327(5964), 449-451.
- 535 Carlson, R.W., Borg, L.E., Gaffney, A.M., Boyet, M., 2013. Rb-Sr, Sm-Nd and Lu-Hf isotope  
 536 systematics of norite 77215: Refining the age and duration of lunar crust formation. XLIV  
 537 Lunar and Planetary Science Conference, Houston Texas. abstract #1621.
- 538 Caro, G. 2011. Early silicate Earth differentiation. *Annual Review of Earth and Planetary*  
 539 *Sciences*, 39, 31-58.
- 540 Clayton, R.N., Onuma, N., Grossman, L., Mayeda, T.K., 1977. Distribution of the pre-solar  
 541 component in Allende and other carbonaceous chondrites, *Earth Planet. Sci. Lett* 34, 209-24.
- 542 Connelly, J.N., Bizzarro, M., Krot, A.N., Nordlund, Å., Wielandt, D., Ivanova, M.A., 2012. The  
 543 absolute chronology and thermal processing of solids in the solar protoplanetary disk.  
 544 *Science* 338, 651-655.
- 545 Connolly, H.C., Burnett, D.S., McKeegan, K.D., 2003. The petrogenesis of type B1 Ca-Al-rich  
 546 inclusions: The spinel perspective. *Meteor. Planet. Sci.* 38, 197-224.
- 547 Davis, A.M., Simon, S.B., Grossman, L., 1992. Melilite composition trends during  
 548 crystallization of Allende Type B1 refractory inclusion melts. XXIII Lunar and Planetary  
 549 Science Conference, Houston Texas. abstract p. 281-282.
- 550 Dunlavey, D. C., Seaborg, G. T. 1953. Alpha Activity of Sm 146 as Detected with Nuclear  
 551 Emulsions. *Physical Review*, 92(1), 206.
- 552 Friedman, A. M., Milsted, J., Metta, D., Henderson, D., Lerner, J., Harkness, A. L. 1966. Alpha  
 553 Decay Half Lives of  $^{148}\text{Gd}$   $^{150}\text{Gd}$  and  $^{146}\text{Sm}$ . *Radiochim. Acta*, 5(4), 192-194.
- 554 Galer, S.J.G., Lugmair, G.W., 1996. Lead isotope systematics of noncumulate eucrites. 60<sup>th</sup>  
 555 Meeting of the Meteoritical Society. Maui, Hawaii. A47-A48.
- 556 Gray, C.M., Papanastassiou, D.A., Wasserburg, G.J., 1973. The identification of early  
 557 condensates from the solar nebula. *Icarus*, 20, 213-239.
- 558 Hans, U., Kleine, T., Bourdon, B., 2013. Rb-Sr chronology of volatile depletion in differentiated  
 559 protoplanets: BABI, ADOR and ALL revisited. *Earth Planet. Sci. Lett.* 374, 204-214.
- 560 Hood, L.L., Ciesla, F.J., Artemieva, N.A., Marzari, F., Weidenschilling, S.J., 2009. Nebular  
 561 shock waves generated by planetesimals passing through Jovian resonances: Possible sites  
 562 for chondrule formation. *Meteorit. Planet. Sci.*, 44, 327-342.
- 563 Jacobsen, B., Matzel J., Hutcheon, I.D., Krot, A.N., Yin, Q.-Z., Nagashima K., Ramon E.C.,  
 564 Weber P. K., Ishii, H.A., Ciesla F.J. 2011. Formation of the short-lived radionuclide  $^{36}\text{Cl}$  in  
 565 the protoplanetary disk during late-stage irradiation of a volatile-rich reservoir. *Astrophys. J.*  
 566 *Lett.* 731. L28-L34.
- 567 Jacobsen, B., Yin, Q.-Z., Moynier, F., Amelin, Y., Krot, A.N., Nagashima, K., Hutcheon, I.D.,  
 568 Palme, H., 2008.  $^{26}\text{Al}$   $^{26}\text{Mg}$  and  $^{207}\text{Pb}$   $^{206}\text{Pb}$  systematics of Allende CAIs: Canonical solar  
 569 initial  $^{26}\text{Al}/^{27}\text{Al}$  ratio reinstated. *Earth Planet. Sci. Lett.* 272, 353-364.
- 570 Jacobsen, S.B., Wasserburg, G.J., 1984. Sm-Nd isotopic evolution of chondrites and achondrites,  
 571 II. *Earth Planet. Sci. Lett.* 67, 137-150.

- 572 Jacobsen, S.B., Wasserburg, G.J., 1980. Sm-Nd isotopic evolution of chondrites. *Earth Planet.*  
573 *Sci. Lett.*, 50, 139-155.
- 574 Kinoshita, N., Paul, M., Kashiv, Y., Collon, P., Deibel, C.M., DiGiovine, B., Greene, J.P.,  
575 Henderson, D.J., Jiang, C.L., Marley, S.T., Nakanishi, T., Pardo, R.C., Rehm, K.E.,  
576 Roberston, D., Scott, R., Schmitt, C., Tang, X.D., Vondrasek, R., Yokoyama, A., 2012. A  
577 shorter  $^{146}\text{Sm}$  half-life measured and implications for  $^{146}\text{Sm}$ - $^{142}\text{Nd}$  chronology in the Solar  
578 System. *Science* 335, 1614-1617.
- 579 Ludwig, K. R. 2009. *Isoplot 4.1*. A Geochronological Toolkit for Microsoft Excel. Berkeley  
580 Geochronology Center, Berkeley.
- 581 Lugmair, G.W., Galer, S.J.G., 1992. Age and isotopic relationships among the angrites Lewis  
582 Cliff 86010 and Angra dos Reis. *Geochim. Cosmochim. Acta.* 56, 1673–1694.
- 583 Lugmair, G.W., Galer, S.G.J., Carlson, R.W., 1991. Isotope systematics of cumulate Eucrite,  
584 EET-87520. *Meteorit. Planet. Sci. Supp.* 26, abstract p. 368.
- 585 Lugmair, G.W., Marti, K., 1977. Sm-Nd-Pu timepieces in the Angra dos Reis meteorite. *Earth*  
586 *Planet. Sci. Lett.*, 35, 273-284.
- 587 Marks, N.A., Borg, L.E., Gaffney, A.M., 2014. Evidence for young anorthositic magmatism on  
588 the Moon from Sm-Nd isotopic measurements for ferroan anorthosite clast 3A from breccia  
589 60016. XLV Lunar and Planetary Science Conference, Houston Texas. abstract #1129.
- 590 Meissner, F., Schmidt-Ott, W. D., Ziegeler, L. 1987. Half-life and  $\alpha$ -ray energy of  $^{146}\text{Sm}$ .  
591 *Zeitschrift für Physik A Atomic Nuclei*, 327(2), 171-174.
- 592 Moynier, F., Agranier, A., Hezel, D. C., Bouvier, A. 2010. Sr stable isotope composition of  
593 Earth, the Moon, Mars, Vesta and meteorites. *Earth and Planetary Science Letters*, 300(3),  
594 359-366.
- 595 Nurmia, M., Graeffe, G., Valli, K., Aaltonen, J. 1964. Alpha activity of Sm-146. Univ. of  
596 Helsinki.
- 597 Nyquist, L.E., Bansal, B., Wiesmann, H., Shih, C.-Y., 1994. Neodymium, strontium and  
598 chromium isotopic studies of the LEW86010 and Angra dos Reis meteorites and the  
599 chronology of the angrite parent body. *Meteor. Planet. Sci.* 29, 872–885.
- 600 Nyquist, L., Bogard, D., Takeda, H., Bansal, B., Wiesmann, H., & Shih, C. Y. (1997a).  
601 Crystallization, recrystallization, and impact-metamorphic ages of eucrites Y792510 and  
602 Y791186. *Geochimica et cosmochimica acta*, 61(10), 2119-2138.
- 603 Nyquist, L.E., Reese, Y.D., Wiesmann, H., Shih, C.-Y., 1999. Two ages for Ibitira: A record of  
604 crystallization and recrystallization?. *Meteorit. Planet. Sci. Supp.* 34, abstract p. 87.
- 605 Nyquist, L.E., Shih, C.-Y., Reese, Y.D., 2008. Sm-Nd for norite 78236 and eucrite  
606 Y980318/433: Implications for planetary and solar system processes. XXXIX Lunar and  
607 Planetary Science Conference, Houston Texas. abstract #1437.
- 608 Nyquist, L.E., Takeda, H., Shih, C.-Y., Wiesmann, H., 2004. Sm-Nd Age and Initial  $^{87}\text{Sr}/^{86}\text{Sr}$   
609 for Yamato 980318: An Old Cumulate Eucrite. XXXV Lunar and Planetary Science  
610 Conference, Houston Texas. abstract p. 1330-1331).

- 611 Nyquist, L.E., Wiesmann, H., Reese, Y., Shih, C.-Y., Borg, L.E., 1997b. Samarium-neodymium  
612 age and manganese-chromium systematics of eucrite Elephant Moraine 90020. Meteorit.  
613 Planet. Sci. Supp. 32, abstract p. 101.
- 614 Papanastassiou, D.A., Ngo, H.H., Wasserburg, G.J., 1987. Sm-Nd systematics in coarse-grained  
615 refractory inclusions from Allende. XVIII Lunar and Planetary Science Conference, Houston  
616 Texas. abstract p. 760-761.
- 617 Papanastassiou, D.A., Wasserburg, G.J., 1969. Initial strontium isotopic abundances and the  
618 resolution of small time differences in the formation of planetary objects. Earth Planet. Sci.  
619 Lett. 5, 361-376.
- 620 Podosek, F.A., Zinner, E.K., Macpherson, G.J., Lundberg, L.L., Brannon, J.C., Fahey, A.J.,  
621 1991. Correlated study of initial  $^{87}\text{Sr}/^{86}\text{Sr}$  and Al-Mg isotopic systematics and petrologic  
622 properties in a suite of refractory inclusions from the Allende meteorite. Geochim.  
623 Cosmochim. Acta 55, 1083-1110.
- 624 Prinzhofer, A., Papanastassiou, D.A., Wasserburg, G.J., 1992. Samarium-neodymium evolution  
625 of meteorites. Geochim. Cosmochim. Acta 56, 797-815.
- 626 Qin L., Carlson R. W. and Alexander C. M. O. D., 2011. Correlated nucleosynthetic isotopic  
627 variability in Cr, Sr, Ba, Sm, Nd and Hf in Murchison and QUE 97008. Geochim.  
628 Cosmochim. Acta 75, 7806–7828.
- 629 Scott, E.R.D., Krot, A.N. Chondritic Meteorites and the high-temperature nebular origins of their  
630 components, in Vol. 341, Chondrites and the Protoplanetary Disk, A.N. Krot, E.R.D. Scott,  
631 B. Reipurth, Eds. (Astronomical Society of the Pacific, San Francisco, 2007) pp. 15-54.
- 632 Sharma, M., Papanastassiou, D.A., Wasserburg, G.J., 1995. Sm-Nd systematics of a large Eucrite  
633 clast in the Vaca Muerta Mesosiderite and initial Solar System  $^{146}\text{Sm}$  abundances. XXVI  
634 Lunar and Planetary Science Conference, Houston Texas. abstract p. 1271-1272).
- 635 Simon, S.B., Grossman, L., Davis, A.M., 1991. Fassaite composition trends during  
636 crystallization of Allende Type B refractory inclusion melts. Geochim. Cosmochim. Acta 55,  
637 2635-2655.
- 638 Stewart, B.W., Papanastassiou, D.A., Wasserburg, G.J., 1994. Sm-Nd chronology and  
639 petrogenesis of mesosiderites. Geochim. Cosmochim. Acta 58, 3487-3509.
- 640 Tanaka, T., Togashi, S., Kamioka, H., Amakawa, H., Kagami, H., Hamamoto, T., Yuhara, M.,  
641 Orihashi, Y., Yoneda, S., Shimizu, H., Kunimaru, T., Takahashi, K., Yanagi, T., Nakano, T.,  
642 Fujimaki, H., Shinjo, T., Asahara, Y., Tanimizu, M., Drafusanu, C., 2000. JNdi-1: A  
643 neodymium isotopic reference in consistency with LaJolla neodymium. Chem. Geo. 168,  
644 279-281.
- 645 Tatsumoto, M., Unruh, D.M., Desborough, G.A., 1976. U-Th-Pb and Rb-Sr systematics of  
646 Allende and U-Th-Pb systematics of Orgueil. Geochim. Cosmochim. Acta, 40, 617-634.
- 647 Tera, F., Carlson, R. W., Boctor, N. Z. 1997. Radiometric ages of basaltic achondrites and their  
648 relation to the early history of the solar system. Geochimica et cosmochimica acta, 61(8),  
649 1713-1731.
- 650 Wasserburg, G. J., Busso, M., Gallino, R., Nollett, K. M., 2006. Short-lived nuclei in the early  
651 Solar System: Possible AGB sources. Nuclear Physics A, 777, 5-69.

- 652 Wadhwa, M., Lugmair, G. W., 1996. Age of the eucrite “Caldera” from convergence of long-  
653 lived and short-lived chronometers. *Geochim. Cosmochim. Acta*, 60, 4889-4893.
- 654 Wetherill, G. W., Mark, R., Lee-Hu, C., 1973. Chondrites: initial strontium-87/strontium-86  
655 ratios and the early history of the solar system. *Science*, 182, 281-283.
- 656

**Table 1. Al3S4 CAI Sm-Nd isotopic data**

Fraction	Wt (mg)	Sm (ppm)	Sm (ng) <sup>e</sup>	Nd (ppm)	Nd (ng) <sup>e</sup>	$\frac{147\text{Sm}}{144\text{Nd}}$ <sup>a,d</sup>	$\frac{142\text{Nd}}{144\text{Nd}}$ <sup>a,b</sup>	$\frac{143\text{Nd}}{144\text{Nd}}$ <sup>a,b</sup>	$\frac{145\text{Nd}}{144\text{Nd}}$ <sup>a,b</sup>	$\frac{148\text{Nd}}{144\text{Nd}}$ <sup>a,b</sup>	$\frac{150\text{Nd}}{144\text{Nd}}$ <sup>a,b</sup>
Mel-Pyx	70.95	4.202	298	13.54	961	0.18751 ± 19	1.141814 ± 4	0.512332 ± 1	0.348395 ± 1	0.241573 ± 1	0.236430 ± 2
Melilite	142.51	1.936	276	6.852	976	0.17076 ± 17	1.141788 ± 4	0.511825 ± 1	0.348395 ± 1	0.241573 ± 1	0.236442 ± 2
Pyx	11.93	7.26	87	18.91	226	0.23204 ± 52	1.141894 ± 5	0.513665 ± 3	0.348394 ± 1	0.241577 ± 1	0.236433 ± 2
d>3.26	54.23	6.262	340	18.13	983	0.20878 ± 21	1.141849 ± 3	0.512986 ± 1	0.348397 ± 1	0.241568 ± 1	0.236421 ± 2
d<3.26	49.12	2.802	138	9.863	484	0.17172 ± 19	1.141789 ± 11	0.511855 ± 4	0.348395 ± 1	0.241571 ± 3	0.236433 ± 7
Fines	152.82	2.874	44	9.141	1397	0.19006 ± 19	1.141819 ± 4	0.512479 ± 1	0.348397 ± 1	0.241568 ± 1	0.236438 ± 2
JNdi Nd Std (N=37)					500		1.141837 ± 7 <sup>c</sup>	0.512101 ± 7 <sup>c</sup>	0.348402 ± 4	0.241578 ± 5	0.236456 ± 6

Abbreviations for mineral fractions are as follows: Mel. = melilite, Pyx = pyroxene, Mel-Pyx = melilite separated from the pyroxene fraction. All samples and standards run as Nd<sup>+</sup>.

<sup>a</sup>. Error limits apply to last digits and include a minimum uncertainty of 0.5% plus 50% of the blank correction for Sm and Nd added quadratically.

<sup>b</sup>. Normalized to  $^{146}\text{Nd}/^{144}\text{Nd} = 0.7219$ . Uncertainties refer to last digits and are  $2\sigma_m$  ( $2 \times$  standard error of measured isotopic ratios).

<sup>c</sup>. Uncertainties refer to last digits and are  $2\sigma_p$  ( $2 \times$  standard deviation of population of mass spectrometry runs on isotopic standard). Isochron are calculated using either using either  $2\sigma_p$  (from standard runs) or  $2\sigma_m$  (from measured isotopic ratios).

<sup>d</sup>.  $^{147}\text{Sm}/^{144}\text{Nd}$  corrected for nucleosynthetic effects using Sm and Nd isotopic compositions measured on 11 bulk Allende CAIs by Brennecka et al. (2011, 2012, 2013). Total effect is < 0.015%.

<sup>e</sup>. Abundances of elements calculated for entire mineral fractions. 95% splits were analyzed for Nd isotopic composition determinations and 5% splits were analyzed for Nd and Sm concentrations.

**Table 2. Al3S4 CAI Rb-Sr isotopic data**

Fraction	Wt (mg)	Rb (ppm) <sup>a</sup>	Rb (ng) <sup>b</sup>	Sr (ppm) <sup>a</sup>	Sr (ng) <sup>b</sup>	<sup>87</sup> Rb/ <sup>86</sup> Sr <sup>a,c</sup>	<sup>87</sup> Sr/ <sup>86</sup> Sr <sup>d</sup>	$\epsilon^{84}\text{Sr} (\pm 2\sigma)^f$
Melilite	142.51	0.064	9.1	242.8	34601	0.00076 ± 1	0.698987 ± 8	0.98±0.19
d<3.26	49.12	0.231	11.3	224.4	11023	0.00298 ± 3	0.699129 ± 8	1.24±0.22
Fines	152.82	0.123	18.8	116.5	17804	0.00305 ± 3	0.699110 ± 8	
Pyx	11.93	0.056	0.7	46.3	553	0.00351 ± 12	0.699152 ± 8	1.34±0.67
Mel-Pyx	70.95	0.234	16.6	115.4	8188	0.00587 ± 6	0.699306 ± 8	1.30±0.21
d>3.26	54.23	0.211	11.5	86.2	4675	0.00709 ± 7	0.699373 ± 8	0.51±0.20
NBS-987 Std (N=49)					~1000		0.710249 ± 9 <sup>c</sup>	

Abbreviations for mineral fractions are as follows: Mel. = melilite, Pyx = pyroxene, Mel-Pyx = melilite separated from the pyroxene fraction. The long term reproducibility of <sup>85</sup>Rb/<sup>87</sup>Rb measured on 30 runs of NBS-984 Rb standard = 2.603 ± 17 and are 2σ<sub>p</sub> (2×standard deviation of population of mass spectrometry runs on isotopic standard) and were used to correct for instrument mass fractionation.

<sup>a</sup> Error limits apply to last digits and include a minimum uncertainty of 1% plus 50% of the blank correction for Rb and Sr added quadratically.

<sup>b</sup> Abundances of elements calculated for entire mineral fractions. 95% splits were analyzed for Rb and Sr concentration determinations and 5% splits were analyzed for Sr isotopic composition.

<sup>c</sup> Uncertainties refer to last digits and are 2σ<sub>p</sub>. (2 x standard deviation of population of mass spectrometry runs on isotopic standard). Isochron are calculated using either 2σ<sub>p</sub> (from standard runs) or 2σ<sub>m</sub> (from measured isotopic ratios), whichever is larger.

<sup>d</sup> Normalized to <sup>86</sup>Sr/<sup>88</sup>Sr = 0.1194. Uncertainties refer to last digits and are 2σ<sub>m</sub> (2×standard error of measured isotopic ratios).

$$f. \quad \epsilon^{84}\text{Sr} = \left( \frac{\left( \frac{\text{Sr}^{84}}{\text{Sr}^{86}} \right)_{\text{sample}}}{\left( \frac{\text{Sr}^{84}}{\text{Sr}^{86}} \right)_{\text{standard}}} - 1 \right) \times 10^4.$$

**Table 3.  $^{146}\text{Sm}$ - $^{142}\text{Nd}$  ages of primitive meteorites and lunar samples calculated using different parameters (Sm-Nd).**

Meteorite/ sample type	Sample Name	Absolute Age (Ma)	Absolute Age Reference <sub>a</sub>	Initial $^{146}\text{Sm}/^{144}\text{Sm}$	Sm-Nd age <sup>b</sup> (Ma)			Sm-Nd age <sup>c</sup> (Ma)			Sm-Nd age <sup>d</sup> (Ma)			$^{146}\text{Sm}$ - $^{142}\text{Nd}$ Reference
					(+)	(-)		(+)	(-)		(+)	(-)		
CV3	CAI	4567.1 ± 0.9			≅4567			≅4567			4555	5	5	
Angrites	LEW 86010	4558 ± 0.5	Pb-Pb <sup>1</sup>	0.0076±0.0009	4554	19	17	4559	12	11	4546	12	11	Nyquist et al., 1994
	LEW 86010	4558 ± 0.5	Pb-Pb <sup>1</sup>	0.0071±0.0017	4544	41	32	4552	27	21	4539	27	21	Nyquist et al., 1994
Euclrites	Angra dos Reis	4512 ± 85	Sm-Nd <sup>2</sup>	0.0063±0.0017	4527	47	35	4540	31	23	4528	31	23	Lugmair & Marti (1977)
	Caldera	4544 ± 19	Sm-Nd <sup>5</sup>	0.0074±0.0013	4549	29	25	4555	19	16	4543	19	16	Wadhwa & Lugmair (1996)
	EET87520	4547 ± 9	Sm-Nd <sup>6</sup>	0.0069±0.0045	4540	157	75	4549	104	49	4537	104	49	Lugmair et al. (1991)
	EET90020	4482 ± 30	Sm-Nd <sup>7,8</sup>	0.0048±0.0020	4486	80	52	4514	53	34	4501	53	34	Nyquist et al. (1997a, 1997b)
	Ibitira	4557.4 ± 0.55	Pb-Pb <sup>9</sup>	0.0091±0.0028	4580	55	40	4576	36	26	4563	36	26	Prinzhofer et al. (1992)
	Ibitira	4557.4 ± 0.55	Pb-Pb <sup>9</sup>	0.0082±0.0008	4566	15	14	4566	10	9	4554	10	9	Nyquist et al. (1999)
	Moama	4466 ± 42	Sm-Nd <sup>3</sup>	0.0041±0.0013	4463	57	41	4498	37	27	4486	37	27	Jacobsen and Wasserburg (1984)
	Moore county	4484 ± 19	Pb-Pb <sup>10</sup>	0.0066±0.0012	4533	30	25	4545	20	16	4532	20	16	Boyet et al. (2010)
Mesosiderite	Y980318	4567 ± 24	Sm-Nd <sup>11</sup>	0.0060±0.0009	4519	24	21	4535	16	14	4523	16	14	Nyquist et al. (2004); Nyquist et al. (1995)
	Y980433	4542 ± 42	Sm-Nd <sup>12</sup>	0.0057±0.0005	4512	14	12	4530	9	8	4518	9	8	Nyquist et al. 1994
	Mt. Padbury	4494 ± 45	Sm-Nd <sup>14</sup>	0.0056±0.0008	4509	22	19	4529	15	13	4516	15	13	Stewart et al (1994)
	Acapulco	4556.4 ± 3	Pb-Pb <sup>16</sup>	0.0070±0.0018	4542	43	34	4551	29	22	4538	29	22	Prinzhofer et al. (1992)
	Lunar	Lunar 60025	4359 ± 3	Pb-Pb <sup>17</sup>	0.0016±0.0003	4321	33	27	4405	22	18	4392	22	18
Lunar 60016	4300 ± 32	Sm-Nd <sup>18</sup>	0.0003±0.0001	4298	60	102	4389	40	67	4377	40	67	Marks et al. (2014)	
Lunar 76535	4307 ± 11	Sm-Nd <sup>19</sup>	0.0014±0.0003	4300	36	29	4391	24	19	4378	24	19	Borg et al. (2013)	
Lunar 77215	4283 ± 23	Sm-Nd <sup>20</sup>	0.0019±0.0009	4351	97	58	4424	64	38	4412	64	38	Carlson et al. (2013)	

All  $^{146}\text{Sm}$ - $^{142}\text{Nd}$  ages calculated from reference age of CAI of 4567 Ma. Absolute ages are either Pb-Pb or  $^{147}\text{Sm}$ - $^{143}\text{Nd}$ . (+) and (-) values represent two standard deviations. Samples with ages older than 4567 Ma are not plotted in Figure 4.

- 1 Lugmair and Galer, (1992); 2 Lugmair & Marti (1977); 3 Jacobsen & Wasserburg (1984); 4 Boyet et al. (2010) 5 Wadhwa & Lugmair (1996); 6 Lugmair et al. (1991); 7,8 Nyquist et al. (1997a, 1997b); 9 Amelin et al. (2006); 10 Tera et al. (1997); 11 Nyquist et al. (2004); Nyquist et al. (2008); 12 Nyquist et al. (1994); 13 Prinzhofer et al. (1992); 14 Stewart et al. (1994); 15 Sharma et al. (1995); 16 Amelin et al. (2005); 17 Borg et al. (2011); 18 Marks et al. (2014); 19 Borg et al. (2013); 20 Carlson et al. (2013)
- $^{146}\text{Sm}$   $t_{1/2}$  = 103 Ma,  $^{146}\text{Sm}/^{144}\text{Sm}$  = 0.00828.
- $^{146}\text{Sm}$   $t_{1/2}$  = 68 Ma,  $^{146}\text{Sm}/^{144}\text{Sm}$  = 0.00828.
- $^{146}\text{Sm}$   $t_{1/2}$  = 68 Ma,  $^{146}\text{Sm}/^{144}\text{Sm}$  = 0.0094.

## Figure Captions:

**Figure 1.** Photomicrograph of Allende CAI Al3S4 from Clayton et al. (1977). The outer 1.5 mm border consists of radially oriented melilite crystals, with spinel content increasing inwards. The interior of the inclusion is primarily crystalline clinopyroxene, melilite, and anorthite with included euhedral spinel. Field of view is 22mm x 17mm.

**Figure 2.** A  $^{147}\text{Sm}$ - $^{143}\text{Nd}$  isochron plot of mineral fractions from Allende CAI Al3S4 yielding an age of  $4560 \pm 34$  million years and an initial  $^{143}\text{Nd}/^{144}\text{Nd}$  of  $0.506657 \pm 43$ . Isochron has a mean squared weighted derivative of 2.4. The Fines fraction is plotted as an open symbol and is excluded from the regression. Inset represents deviation of individual points from the isochron in epsilon units:

$$\epsilon^{143} = \left( \frac{\left( \frac{\text{Nd}^{143}}{\text{Nd}^{144}} \right)^{\text{sample}}}{\left( \frac{\text{Nd}^{143}}{\text{Nd}^{144}} \right)^{\text{standard}}} - 1 \right) \times 10^4.$$

**Figure 3.** A  $^{146}\text{Sm}$ - $^{142}\text{Nd}$  isochron plot of mineral fractions from Allende CAI Al3S4. The slope of this isochron yields an initial  $^{146}\text{Sm}/^{144}\text{Sm}$  ratio of the Solar System of  $0.00828 \pm 0.00044$ . The y-intercept defines an initial  $^{142}\text{Nd}/^{144}\text{Nd}$  ratio of  $1.141496 \pm 0.000018$  ( $\epsilon^{142}\text{Nd} = -3.01 \pm 0.16$ ), which is in good agreement with the initial  $^{142}\text{Nd}/^{144}\text{Nd}$  ratios calculated for both chondritic meteorites ( $\epsilon^{142}\text{Nd} = -3.13 \pm 0.07$ ; Boyet et al., 2005) and Earth from our Nd standard ( $\epsilon^{142}\text{Nd} = -2.92 \pm 0.07$ ) using  $^{147}\text{Sm}/^{144}\text{Nd} = 0.1960$  to  $0.1967$  (Bouvier et al., 2008; Jacobsen and Wasserburg, 1980, 1984) and assuming a half-life of  $^{146}\text{Sm} = 103$  Ma. Inset represents deviation of individual points from the isochron in epsilon units:

$$\epsilon^{142} = \left( \frac{\left( \frac{\text{Nd}^{142}}{\text{Nd}^{144}} \right)^{\text{sample}}}{\left( \frac{\text{Nd}^{142}}{\text{Nd}^{144}} \right)^{\text{standard}}} - 1 \right) \times 10^4.$$

**Figure 4.** Comparison of  $^{146}\text{Sm}$ - $^{142}\text{Nd}$  ages and Pb-Pb and  $^{147}\text{Sm}$ - $^{143}\text{Nd}$  ages. The  $^{146}\text{Sm}$ - $^{142}\text{Nd}$  ages are calculated assuming A)  $^{146}\text{Sm}$   $t_{1/2} = 103$  Ma and initial solar system  $^{146}\text{Sm}/^{144}\text{Sm} = 0.00828$  (filled circles), B)  $^{146}\text{Sm}$   $t_{1/2} = 68$  Ma and initial solar system  $^{146}\text{Sm}/^{144}\text{Sm} = 0.0094$  (gray triangles), and C)  $^{146}\text{Sm}$   $t_{1/2} = 68$  Ma and initial solar system  $^{146}\text{Sm}/^{144}\text{Sm} = 0.00828$  (open squares). The lines represent best fits to the data. The regression for the 103 Ma half-life lies closest to the 1:1 line representing perfect agreement between the different chronometers.

**Figure 5.** A  $^{87}\text{Rb}$ - $^{86}\text{Sr}$  isochron plot of Allende CAI Al3S4 mineral fractions yielding an age of  $4247 \pm 110$  million years. Age calculated using a decay constant of  $\lambda=0.01402 \text{ Ga}^{-1}$  (Begemann et al., 2001). The Fines fraction is plotted as an open symbol and is excluded from the regression. Inset represents deviation of individual points from the isochron in epsilon units

$$\epsilon^{87} = \left( \frac{\left( \frac{\text{Sr}^{87}}{\text{Sr}^{86}} \right)^{\text{sample}}}{\left( \frac{\text{Sr}^{87}}{\text{Sr}^{86}} \right)^{\text{standard}}} - 1 \right) \times 10^4.$$

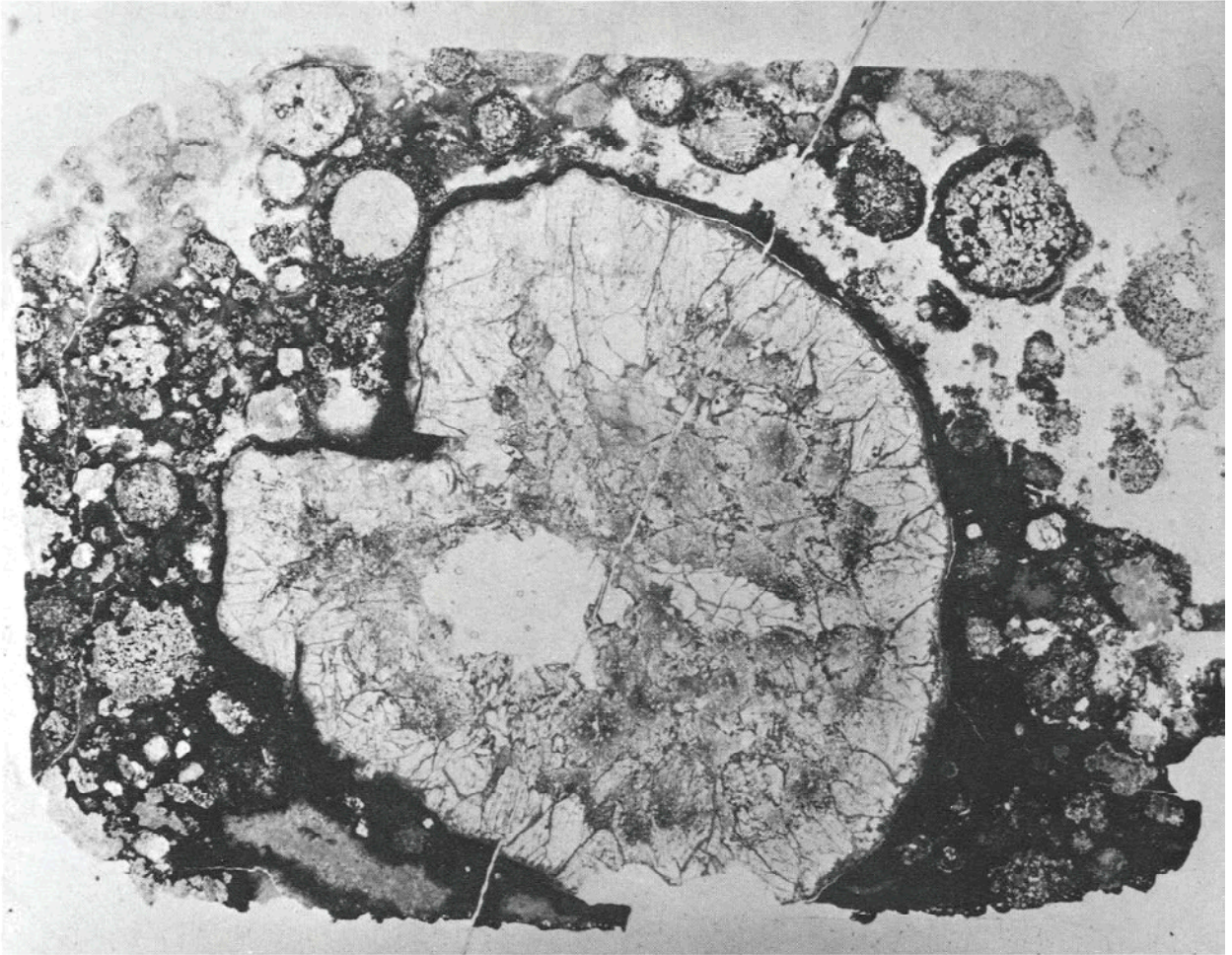


Figure 1.

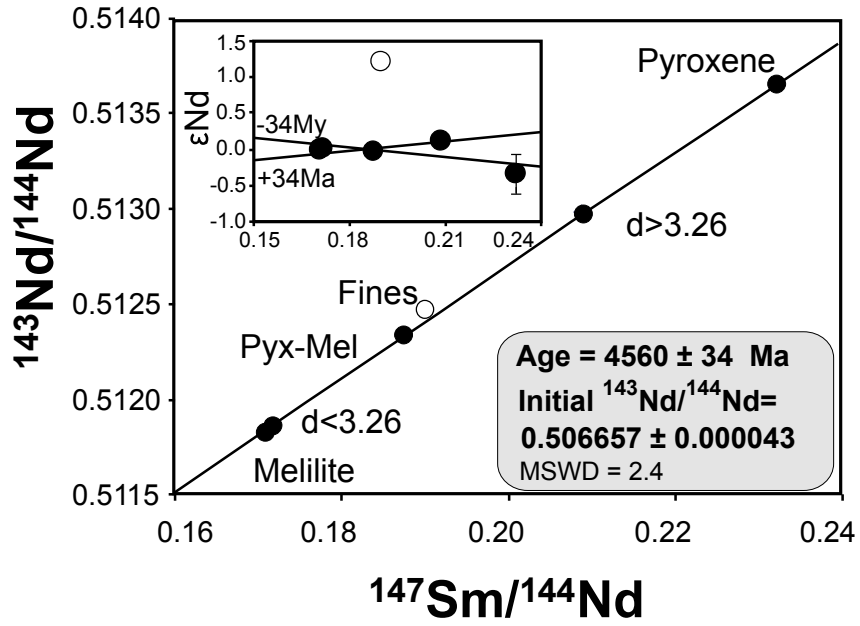


Figure 2.

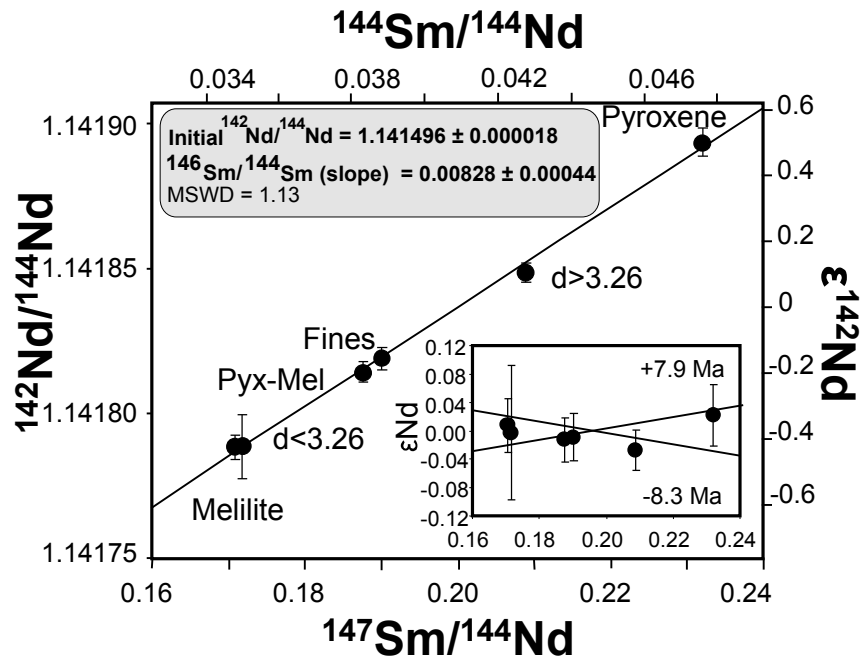
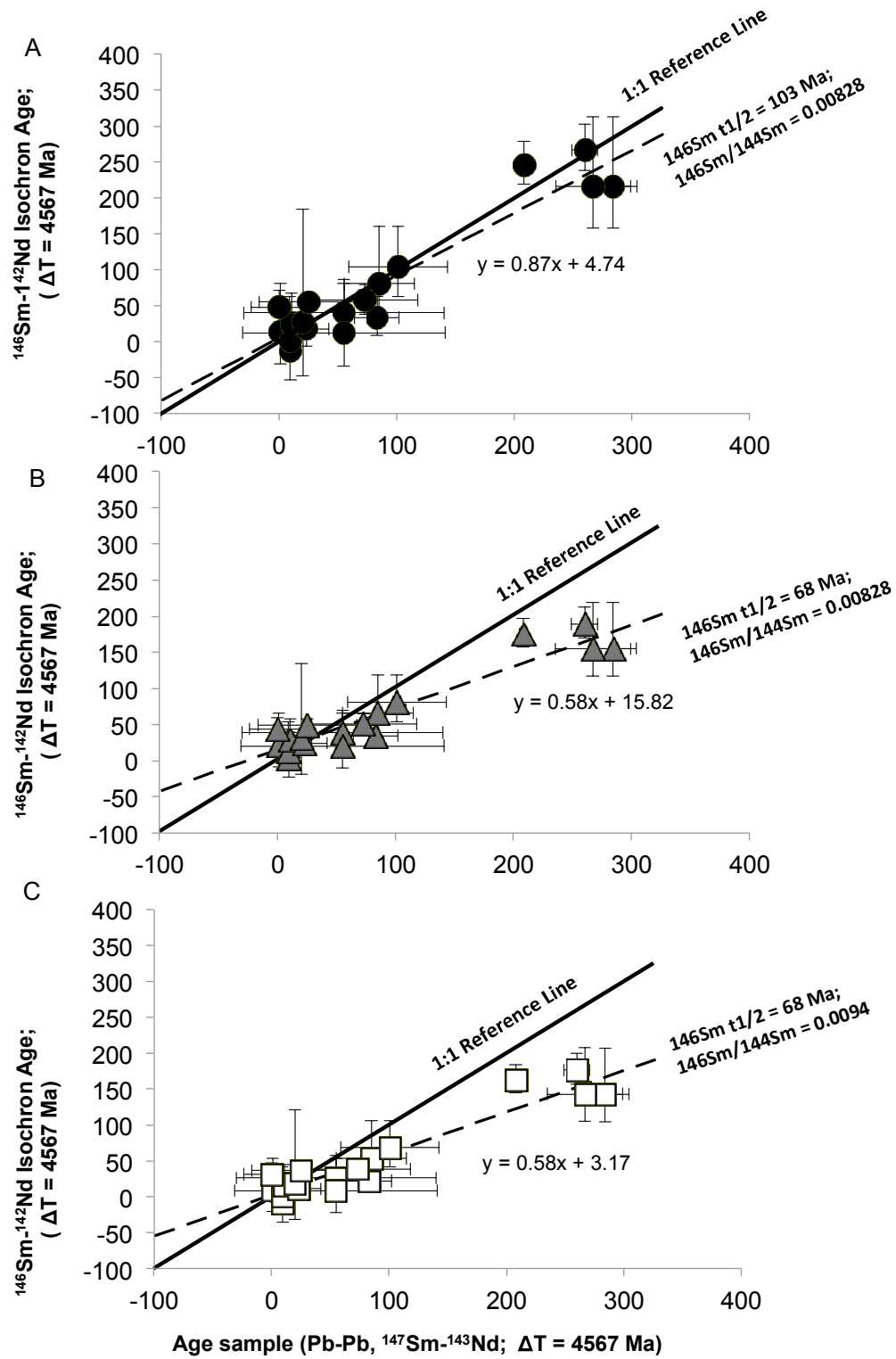


Figure 3.



**Figure 4.**

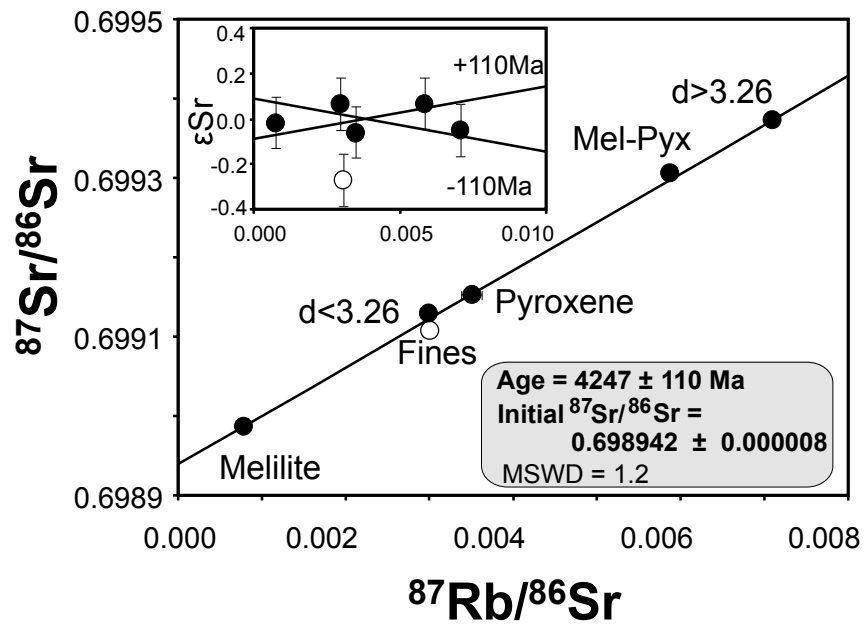


Figure 5.